Benchmarking Reclaimed M247 Powder Against Conventionally Sourced Stainless Powders for Metal Additive Manufacturing

FEBRUARY 2026

RICE UNIVERSITY

Rice University - Particle Flow and Tribology Lab
George R. Brown School of Engineering

Wesley D. Combs
C. Fred Higgs III, Ph.D.

Table of Contents

Introduction

There is a growing interest in the use of powder reclamation within the powder bed additive manufacturing (PBAM) industry. Powders are considered reclaimed if they are sourced from scrap material [1, 2, 3]. Most PBAM parts are constructed from feedstock powders retrieved by traditional means, including mining, melting, and atomization. Regardless of the material sourcing method used, both powder bed fusion and binder jetting, the two general types of PBAM methods, build parts by using feedstock powder within a layerwise, build-up scheme that alternates between powder recoating and densification. The goal of powder recoating is to supply a smooth, dense layer of powder onto the build plate for subsequent densification either by melting or liquid binding [4, 5]. Near-net-shape, highly dense parts with low surface roughness can be constructed with high probability if the recoating step is successful. Feedstock powders with low cohesion and high particle mobility (flowability) have the least stringent printing requirements to establish a high-quality layer spreading process. For example, powders with inherently high flowability do not need minimal spreading speeds, maximal layer thicknesses, substantial hopper oscillation, flow additives, particle surface treatment, air fluidization, or extremely precise moisture control. As a result, using these powders in PBAM printers reduces overall costs related to trial-and-error printing and printing process modification.

Powder surface chemistry, particle size distribution, and particle shape are among the most important factors affecting powder spreadability, all heavily influenced by the powder production technique. Atomization feedstock materials are traditionally retrieved through ore mining. This extraction process is not only expensive in terms of financial resources and time [6, 7], but it is also one of the key contributors to the carbon footprint associated with PBAM product life cycles. Historically, most parts printed from powder bed fusion and binder jetting technologies consist of powders atomized from fresh metal extractions. However, powder reclamation can significantly reduce the product carbon footprint and material costs by leveraging scrap metal parts from decommissioned systems and failed prints through repeated melting and atomization [8, 9]. Excessively coarse particles produced from the atomization process can also be reclaimed within this method of part production, known as circular manufacturing [10]. Essentially, waste material is continuously melted and atomized to yield reclaimed feedstock powder.

The powder reclamation process is especially beneficial when printing with a material of high intrinsic value. This study provides an example of such a case with M247 nickel powder and compares its powder rheological behavior and additive manufacturing suit-ability to that of 2205 and 316 stainless steel powders. Recommendations on the layer thickness and spreading speed of the powder recoating phase can be derived from the analysis of powder flow at varying stress levels and strain rates using powder rheology [11, 12, 13]. Traditional techniques such as the angle of repose [14, 15, 16] and shear cell testing [17, 18], as well as modern methodologies such as rotating drum experiments [19, 20], have become standard elements in academic and corporate additive manufacturing suitability analysis. This study observes the flowability (the ease of relative particle motion) and cohesion (a measure of interparticle attraction) of one reclaimed powder and two conventionally sourced powders according to a suite of tests provided by the FT4 powder rheometer, commonly deployed for PBAM applications [21, 22, 23, 24]. Implementing newer materials like M247 into an AM pipeline can be challenging. Therefore, benchmarking the flowability and additive manufacturing suitability of M247 against conventionally sourced powders that are commonly used in AM, such as stainless steel, can inform printing parameter modifications. Additionally, the feasibility of high-quality circular manufacturing with M247 (and other reclaimed metal powders) is strengthened by its superior powder flow performance in comparison to 2205 and 316 stainless steel, demonstrating that powder reclamation does not necessarily reduce powder flowability or AM suitability.

Material & Methods

The powder flowabilities of three different metals, one nickel superalloy (OptiPowder M247) and two steel powders (2205 and 316), were measured in this study. OptiPowder M247 (Continuum Powders, USA) is 100% reclaimed powder and is sourced from scrap metal parts of the same alloy. Scrap parts are converted into powder using a proprietary method involving plasma torch melting within a cold hearth for purity control followed by fully inert horizontal gas atomization to prevent contamination. 2205 stainless steel (Sandvik, U.K.) and 316 (Desktop Metal, U.S.A.) are both gas-atomized with nitrogen as the inert gas. Particle size distribution and density measurements for each material are shown in Table 1.

Table 1: Particle size percentiles (D_{10}, $D_{50,}$ and D_{90}), PSD width (*span*), and conditioned bulk density (ρ_c).

Material	D_{10}(µm)	D_{50}(µm)	D_{90}(µm)	Span	S_w	ρ_c (g/cm³)
M247	7.44	18.2	48.4	2.25	3.15	5.49
2205	7.60	24.3	53.4	1.88	3.02	4.31
316	7.60	29.9	43.5	1.20	3.38	4.52

The FT4 powder rheometer, a universal powder flow tester, was used to conduct a battery of characterization tests on the three metal powders. The rheometer provides three types of tests: dynamic flow, bulk, and shear. This work covers examples from the dynamic flow and bulk methodologies. One of the dynamic flow tests is called the stability and variable flow rate test (SVFR), and it centers on measuring resistance to blade circulation within a powder bed. The following equation is used to determine flow energy (resistance) $E=\int_o^H T/R \tan(\alpha) + F)\, dh$, where *E* is the total energy, *T* is the torque experienced by the blade, *R* is the blade's radius, *α* is the helix angle, *F* is the axial force experienced by the blade, and H is the height of the powder column. The SVFR test consists of seven test cycles at blade tip speeds of 100 mm/s (stability region) and four test cycles at blade tip speeds of 100, 70, 40, and then 10 mm/s (variable flow rate region) through a 25 ml powder bed vessel.

Stability of powder flow at constant flow speed is estimated by the stability index, which is the ratio of the stability region's last flow energy to its first flow energy. Another measure of powder flow stability is the flow rate index (*FRI*), which accounts for the change in flow rate by calculating the ratio of flow energy at 10 mm/s blade tip speed to the last flow energy at 100 mm/s blade tip speed. Lastly, powder bulk density (ρ_c) is determined after a pre-conditioning cycle establishes a highly repeatable packing state at the beginning of the SVFR test. The remaining category of FT4 powder rheometer experiments discussed in this study is bulk testing. An example of this type is the compressibility test, which consists of measuring the change in powder column volume (*CPS*) from 10 ml to lower amounts as a function of normal stress imparted by a stainless steel mesh head. Normal stress ranges from 1 to 15 kPa during this test.

Results

Dynamic flow testing

Confined (downward) flow resistances for each of the three metal powders are shown in Fig. 1. The flow energy profiles do not portray erratic behavior and do not exhibit spurious spikes. High flow stability at a constant tip speed can be qualitatively asserted for all materials. Nonetheless, 2205 and 316 exhibit slowly increasing flow resistances as the cycles progress, whereas M247 remains relatively constant. Positive slopes in consumed energy within the stability region, albeit small in magnitude, could be caused by limited moisture exposure, particle attrition, or plastic deformation. It is quite apparent that the blade consumes the most energy when traversing downwards through a column of M247 powder rather than through steel powders. In other words, M247 requires the greatest amount of energy to start powder flow in a confined system. Within the stability region (cycles 1 through 12), 2205 presents greater flow resistance than 316. However, in the variable region (cycles 13 through 17), 316 surpasses 2205 and even approximates the flow energy of M247 at a tip speed of 10 mm/s.

The basic flowability energy (*BFE*) is simply the confined flow resistance of cycle 12, as shown in Fig. 1. M247 possesses a *BFE* around 750 mJ, and the *BFE* values of the remaining two metal powders range from 500 to 600 mJ. Flow energy has an intricate relationship with general flowability and spreadability. Consider two hypothetical powders: Powder A and Powder B. If Powder A and Powder B are very different in terms of their particle size and density, then superior flowability is typically indicated by greater magnitudes of flow resistance. This is because high flow energy is normally associated with coarse and dense particles rather than cohesion. Gravitational forces have a cubic relationship with particle size [25], while cohesive forces showcase a linear correlation with particle size [26]. Therefore, if Powder A has a greater average particle size or density than Powder B, its ratio of gravitational forces to cohesion will be greater than that of Powder B, optimizing flowability and spreadability [27, 28, 29]. Alternatively, flow energy is inversely correlated with flowability when considering powders similar in particle size and density. In this case, if Powder B has a lower flow energy than Powder A, this likely signifies that Powder B experiences less opposition to motion from friction and cohesion due to smoother particle surface topologies, more spherical particle morphologies, or less interparticle attraction due to material [30, 31].

Figure 1: Downward flow energies associated with the SVFR test.

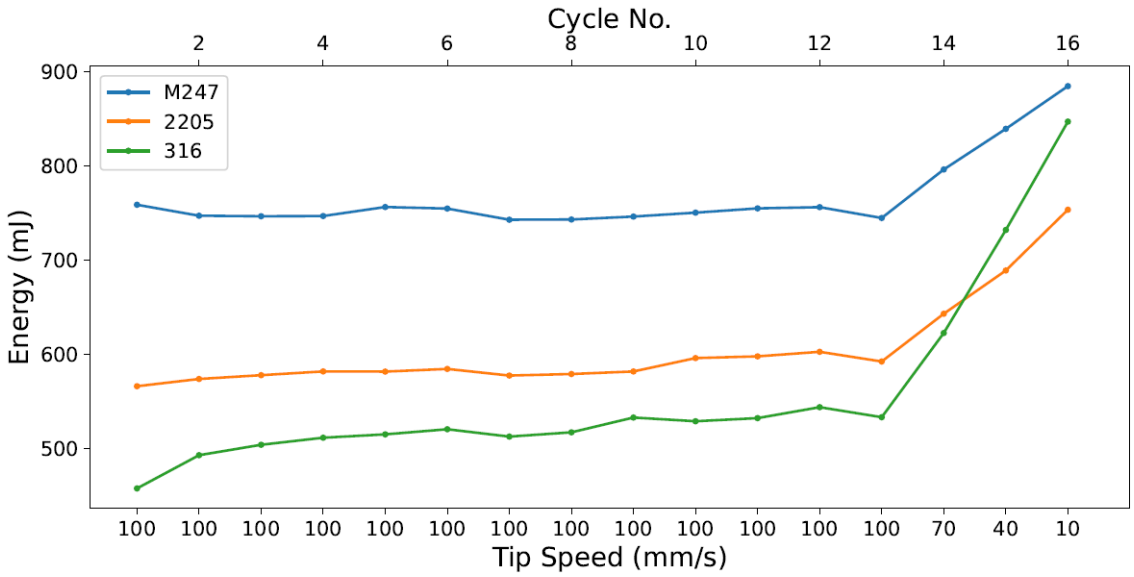

According to Table 1, M247 is the finest of the three powders in terms of mean particle size and moderate in terms of D_{90}. In terms of overall PSD, M247 has the broadest PSD as measured by span and a moderate PSD width according to S_w. Based on particle size, M247 should not exhibit relatively excellent flow properties. However, the high conditioned bulk density (ρ_c) of M247 should play a critical role in increasing its flowability. Due to the significant dissimilarity in powder density, the greater confined flow resistances of M247 in the SVFR test, as shown in Fig. 1, characterize it as having superior flowability over the steel powders. Although M247 will most likely require higher kinetic energy transfer from recoating systems to initiate flow than steel powders, its greater density should correlate with easier powder deposition and less entrapped air.

Flow stability has already been commented on qualitatively, but quantitative results can be seen in Fig. 2. In both the stability and variable region, M247 has the highest flow stability as indicated by the lowest *SI* and *FRI*. M247 nearly attains the ideal stability index value of 1. The powder's very low SI showcases that minimal irreversibilities have been produced by SVFR testing, and its minimal *FRI* indicates that its flow is weakly dependent on the dynamic conditions. 2205 has slightly less flow stability, followed by 316. The AM spreading phase should be easier and more consistent during repeated use and with varying spreader traverse and rotational speeds for M247 than for the steel powders. Additionally, it is expected that M247 would require the lowest refresh rate of all tested powders, since its flow behavior is highly reproducible, reducing the amount of unused conventionally sourced powder material needed for each printing session. In general, M247 should exhibit exemplary AM spreading performance as long as sufficient energy is provided to kickstart flow.

Figure 2: Flow stability indices related to constant flow rate (*SI* : Stability Index) and variable flow rate (*FRI* : Flow Rate Index).

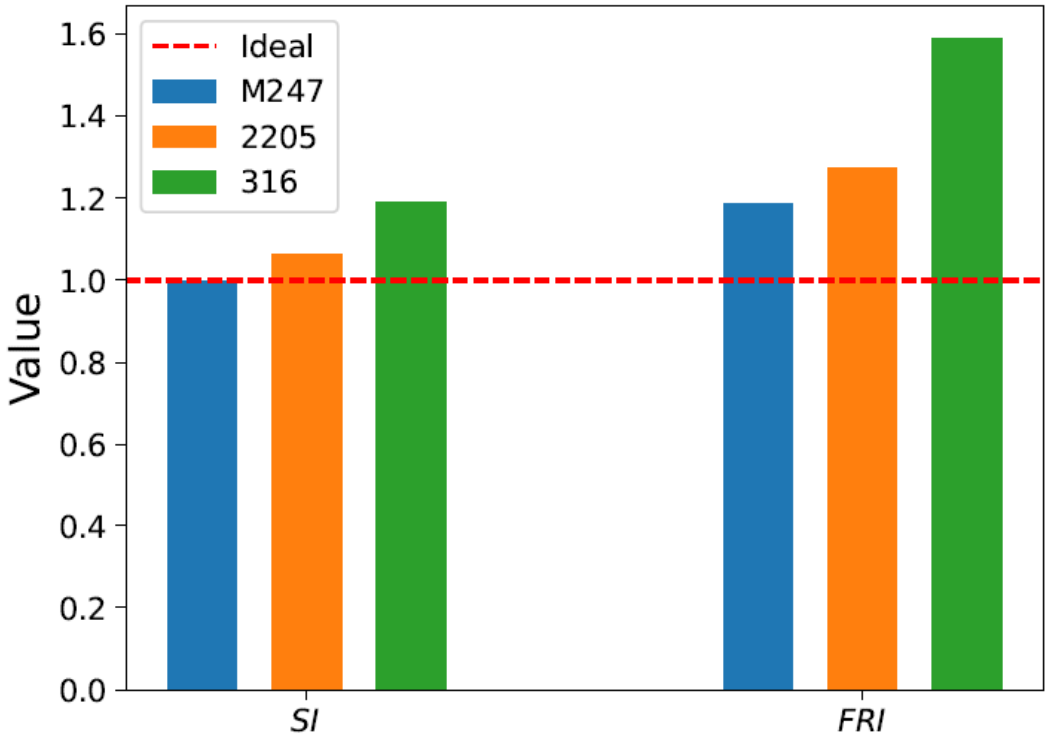

Bulk Testing

Desktop Metal and Freeman Technology developed an AM spreadability classification system (shown as colored regions in Fig. 3) that includes criteria for the compressibility test [32]. This FT4 test is most pertinent to processes such as hopper flow where stress application from machinery or extensive overlying powder layers is present during flow. Insufficient powder compressibility is a sign of potentially poor powder relocation and packing behavior. Excessive compressibility is common among cohesive materials, since these powders tend to trap pockets of air. Because these materials are usually less permeable, entrapped air does not simply vent out of deposited powder, but is instead forced out upon compression. Percent changes in powder column volumes are plotted as functions of compressive stress acting normal to the column in Fig. 3. 316 and 2205 steel powders comfortably reside in the medium to high region, with 316 exhibiting more of a linear relationship with normal stress than 2205. M247 exhibits the lowest compressibility (reaching slightly over 2%) and travels along the boundary between the low to medium and medium to high regions. All materials predominantly occupy the printable regions. Cohesive powders tend to have higher *CPS*. Therefore, flowability is negatively correlated with this test metric. M247 indicates the lowest powder volume change as a result of normal stress, supporting the claim that it possesses a small amount of entrapped air pockets. M247's moderate compressibility also implies that there should be minimal disturbance of underlying layers during recoating compression.

Figure 3: Compressibility percentages (CPS) or volume changes of a powder column as functions of compressive stress. Regions of flowability were determined by extensive AM material testing [30].

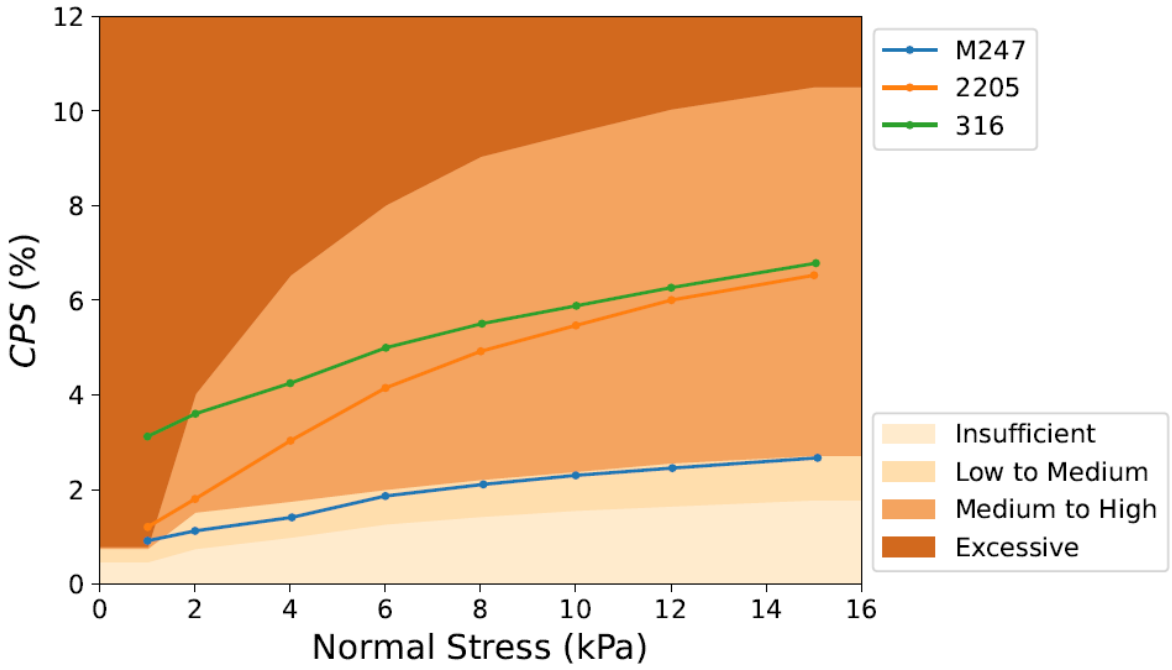

Additive Manufacturing Suitability

Multiple aspects of the PBAM compatibility of various powders have been captured within two major methods. Both methods specifically relate to the powder recoating step and do not provide direct insight into melting or jetting suitability. An aspect of one of these methods was covered in the previous section, and the other method will be discussed here. This AM feasibility assessment technique is known as the additive manufacturing suitability factor (AMS) [33]. The traditional form of this factor is defined as $AMS = (SV^* + CI^*_{15\ kPa} + PD^*_{15\ kPa} + SE^* + AE^*_{10} + BFE^* + c^*)/7$, where SV is the specific volume (the inverse of ρ_c), $CI_{15\ kPa}$ is the compressibility index (ratio of powder density under 15 kPa of normal stress to ρ_c), $PD_{15\ kPa}$ is the pressure drop of air flowing at 2 mm/s across a column that is compressed at 15 kPa, *SE* is the specific energy (flow energy per unit mass for unconfined flow), AE_{10} is the aeration energy (confined flow energy with air flow of 10 mm/s), and *c* is the cohesion parameter from shear cell testing. Each parameter is normalized by the maximum value recorded among the considered materials. As a result, *AMS* ranges from 0 to 1. If the average particle sizes and densities of two powders are similar, the powder with more cohesion tends to exhibit greater flow resistance (*BFE*, *SE*, and AE_{10}), greater density change under compression ($CI_{15\ kPa}$), greater shear strength without compression (*c*), and greater porosity (*SV*). Consequently, optimal spreadability aligns with minimal values for each of the seven *AMS* components shown in Fig. 4.

2205 and 316 powders have similar performance according to $CI_{15\ kPa}{}^*$, c^*, SE^*, and SV^*. For the remaining variables, 316 possessed the lowest flow energies (AE^* and BFE^*) while 2205 exhibited the lowest pressure drop ($PD_{15\ kPa}{}^*$). M247 receives significantly lower *SV*, *SE*, *c*, and $CI_{15\ kPa}$ than 316 and 2205. The compressibility index ($CI_{15\ kPa}{}^*$) is where M247 separates itself from the steel powders by the largest degree in terms of spreadability. The AMS factors are reported in Fig. 5.

Unsurprisingly, M247 receives the lowest (and best) AMS factor slightly above 0.6, while the steel powders' factors are slightly greater than 0.8, with 316 powder slightly outperforming 2205 powder. These findings imply that M247 should be considerably better suited for the powder delivery and spreading phases within PBAM techniques. As was previously demonstrated, the AMS factor is a comparative heuristic and depends on normalization and select powder flow metrics. Regardless, since both 316 and 2205 powders are qualified AM powders that have repeatedly resulted in high-quality parts, the AMS factors indicate that M247 is expected to perform favorably as a feedstock powder for the recoating phase in binder jetting and powder bed fusion printers.

Figure 4: Normalized components of the additive manufacturing suitability factor (*AMS*). Minimal values for each component align with high flowability and spreadability.

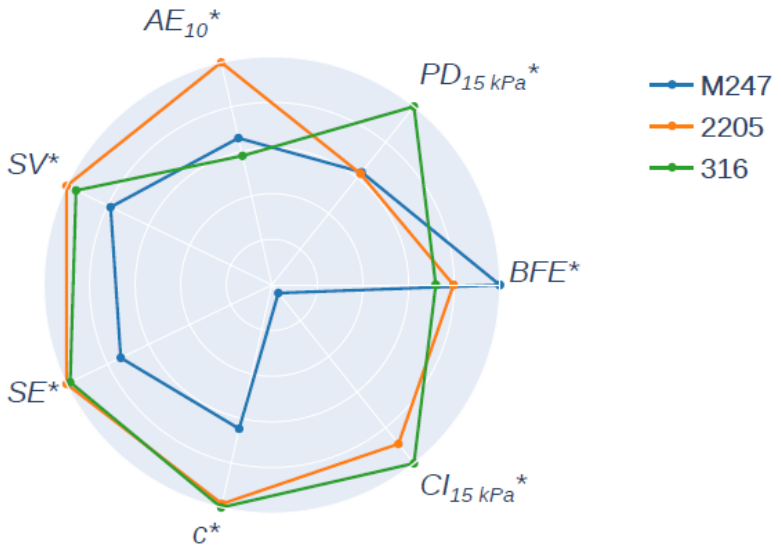

Conclusion

Circular manufacturing provides immense advantages over traditional sourcing techniques for the AM industry. Metal powders, such as those with high nickel concentration, can be entirely produced by atomizing revert scrap material. High-quality parts are then utilized for a prescribed amount of time or until monitored performance worsens below some threshold. These parts are then converted into powder once again, closing the loop of circular manufacturing.

Building ASTM-grade metal parts with M247 and other circular manufacturing powders reduces the product carbon footprint and overall material costs. Although powder reclamation can worsen AM suitability, the powder flow behavior of M247, compared with that of 2205 and 316 steels, shows that a material's intrinsic flowability is not always jeopardized by circular manufacturing. As long as a certain material exhibits excellent flowability, as M247 consistently did across a variety of FT4 powder rheometer tests, reusing scrap parts of that same material only extends its advantages by increasing material efficiency and mitigating international supply chain concerns. M247 powder's excellent flow performance indicates that it is highly likely to provide part suppliers and customers with an easier, more robust, and more consistent AM printing experience. M247 is a dense, moderately sized powder that performed extremely well with respect to various AM applications including but not limited to dynamic stability upon repeated use (*SI*), robustness of flow resistance to various spreading speeds (*FRI*), and weak underlying layer disturbance caused by powder rearrangement under consolidation (*CPS*). Printing recommendations can be made for M247, such as the need for a sufficiently high spreading speed to overcome flow resistance and the relatively light influence of a further increase in printing speeds on powder dynamics.

Figure 5: Additive manufacturing suitability factors (AMS) for each powder. Lower values correlate with better printing feasibility within the powder recoating phase.

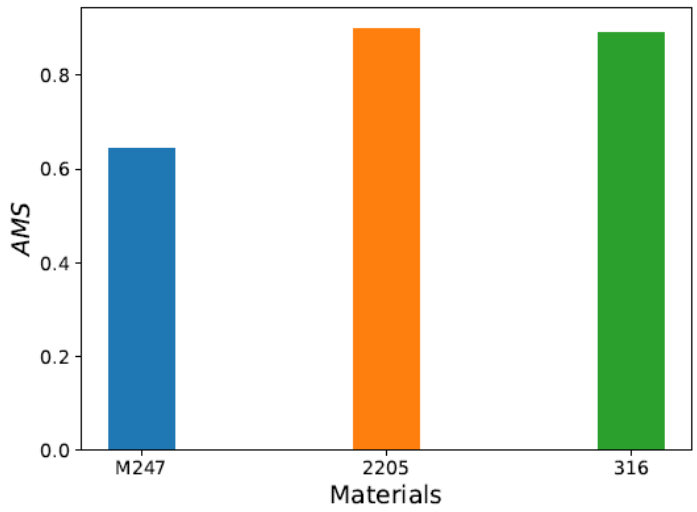

It is worth acknowledging that this work does not include uncertainty bounds for FT4 powder rheometer data, a comparison between steel and nickel powder chemical compositions, or print-scale validation. The aim of this work is simply to investigate the powder rheology of a high-quality reclaimed metal powder and to compare the results with the flow metrics of standard, conventionally sourced AM powders. The *AMS* factor suggests that M247 is better suited for the powder recoating phase within PBAM processes than 316 and 2205 steels. This is mostly due to the very low compressibility index of M247 relative to the steel powders. Overall, M247 powder benefits from high bulk density, resulting in relatively exceptional rheological performance and providing an insightful case study that bolsters the relevancy of circular manufacturing.

Acknowledgments

This material is based upon work supported by the National Science Foundation Graduate Research Fellowship Program under Grant No. 1842494. Any opinions, findings, and conclusions or recommendations expressed in this material are those of the author(s) and do not necessarily reflect the views of the National Science Foundation. This work was also supported by a NASA Space Technology Graduate Research Opportunities Fellowship, United States of America, Grant No. 80NSSC24K1396. The authors gratefully acknowledge the assistance of subject matter experts at Continuum Powders. Also, the authors are thankful for both the allocation of tested materials and technical support from AmPd Labs.

References

[1] Moghimian, P., Poiri´e, T., Habibnejad-Korayem, M., Zavala, J. A., Kroeger, J., Marion, F., and Larouche, F., 2021. "Metal powders in additive manufacturing: A review on reusability and recyclability of common titanium, nickel and aluminum alloys". Additive Manufacturing, 43. https://doi.org/10.1016/j.addma.2021.102017.

[2] Milewski, J. O., 2017. Additive Manufacturing of Metals: From Fundamental Technology to Rocket Nozzles, Medical Implants, and Custom Jewelry. Springer International Publishing.

[3] Gaustad, G., Olivetti, E., and Kirchain, R., 2012. "Improving aluminum recycling: A survey of sorting and impurity removal technologies". Resources, Conservation and Recycling, 58, pp. 79–87. https://doi.org/10.1016/j.resconrec.2011.10.010.

[4] Mostafaei, A., Elliot, A. M., Barnes, J. E., Li, F., Tan, W., Cramer, C. L., Nandwana, P., and Chmielus, M., 2021. "Binder jet 3d printing—process parameters, materials, properties, modeling, and challenges". Progress in Materials Science, 119. https://doi.org/10.1016/j.pmatsci.2020.100707.

[5] Singh, R., Gupta, A., Tripathi, O., Srivastava, S., Singh, B., Awasthi, A., Rajput, S. K., Sonia, P., Singhal, P., and Saxena, K. K., 2020. "Powder bed fusion process in additive manufacturing: An overview". Materials Today: Proceedings, 26, pp. 3058–3070. https://doi.org/10.1016/j.matpr.2020.02.635.

[6] Curry, J. A., Ismay, M. J., and Graeme, J. J., 2014. "Mine operating costs and the potential impacts of energy and grinding". Minerals Engineering, 56, pp. 70–80. https://doi.org/10.1016/j.mineng.2013.10.020.

[7] Fikru, M. G., and Romani, I. G., 2024. Optimizing Mineral Extraction and Processing for the Energy Transition: Evaluating Efficiency in Single versus Joint Production. MIT Center for Energy and Environmental Policy Research.

[8] Landi, D., Spreafico, C., and Russo, D., 2023. "Lca of titanium powder: empirical evidence vs data from patents, possible future applications". Procedia CIRP, 116, pp. 318–323. https://doi.org/10.1016/j.procir.2023.02.054.

[9] Cacace, S., Furlan, V., Sorci, R., Semeraro, Q., and Boccadoro, M., 2020. "Using recycled material to produce gas-atomized metal powders for additive manufacturing processes". Journal of Cleaner Production, 268. https://doi.org/10.1016/j.jclepro.2020.122218.

[10] Raoufi, K., Badwe, S., and Haapala, K. R., 2025. "Improvement of environmental performance of nickel powder production through material circularity". International Design Engineering Technical Conferences and Computers and Information in Engineering Conference. American Society of Mechanical Engineers. https://doi.org/10.1115/DETC2025-169128.

[11] Spierings, A. B., Voegtlin, M., Bauer, T., andWegener, K., 2016. "Powder flowability characterisation methodology for powder-bed-based metal additive manufacturing". Progress in Additive Manufacturing, 1, pp. 9–20. https://doi.org/10.1007/s40964-015-0001-4.

[12] Baesso, I., Karl, D., Spitzer, A., Gurlo, A., G¨unster, J., and Zocca, A., 2021. "Characterization of powder flow behavior for additive manufacturing". Additive Manufacturing, 47. https://doi.org/10.1016/j.addma.2021.102250.

[13] Mehrabi, M., Gardy, J., Talebi, F. A., Farshchi, A., Hassanpour, A., and Bayly, A. E., 2023. "An investigation of the effect of powder flowability on the powder spreading in additive manufacturing". Powder Technology, 413. https://doi.org/10.1016/j.powtec.2022.117997.

[14] Al-Hashemi, H. M. B., and Al-Amoudi, O. S. B., 2018. "A review on the angle of repose of granular materials". Powder Technology, 330, pp. 397–417. https://doi.org/10.1016/j.powtec.2018.02.003.

[15] Meier, C., Weissbach, R., Weinberg, J., Wall, W. A., and Hart, A. J., 2019. "Modeling and characterization of cohesion in fine metal powders with a focus on additive manufacturing process simulations". Powder Technology, 343, pp. 855–866. https://doi.org/10.1016/j.powtec.2018.11.072.

[16] Wagner, J. J., and Higgs III, C. F., 2024. "Coupled cfd-dem simulation of interfacial fluid–particle interaction during binder jet 3d printing". Computer Methods in Applied Mechanics and Engineering, 421, pp. 855–866. https://doi.org/10.1016/j.cma.2024.116747.

[17] Lanzerstorfer, C., 2025. "Flow properties of additive manufacturing metal powders: influencing parameters and wall friction reduction by diamond-like carbon coating". The International Journal of Advanced Manufacturing Technology, 136, pp. 5427–5435. https://doi.org/10.1007/s00170-025-15175-w.

[18] Zegzulka, J., Gelnar, D., Jezerska, L., Prokes, R., and Rozbroj, J., 2020. "Characterization and flowability methods for metal powders". Scientific reports, 10(1). https://doi.org/10.1038/s41598-020-77974-3.

[19] Tondare, V. N., Whiting, J. G., Pintar, A. L., Moylan, S. P., Neveu, A., and Francqui, F., 2024. "An interlaboratory study for assessing repeatability and reproducibility of the data generated by rotating drum powder rheometers (part 1: Granudrum)". Powder Technology, 441. https://doi.org/10.1016/j.powtec.2024.119810.

[20] Espiritu, E. R. L., Kumar, A., Nommeotts-Nomm, A., Lerma, J. A. M., and Brochu, M., 2020. "Investigation of the rotating drum technique to characterise powder flow in controlled and low pressure environments". Powder Technology, 366. https://doi.org/10.1016/j.powtec.2020.03.029.

[21] Strondl, A., Lyckfeldt, O., Brodin, H., and Ackelid, U., 2015. "Characterization and control of powder properties for additive manufacturing". Jom, 67, pp. 549–554. https://doi.org/10.1007/s11837-015-1304-0.

[22] Clayton, J., Millington-Smith, D., and Armstrong, B., 2015. "The application of powder rheology in additive manufacturing". Jom, 67, pp. 544–548. https://doi.org/10.1007/s11837-015-1293-z.

[23] Brika, S. E., Letenneur, M., Dion, C. A., and Brailovski, V., 2020. “Influence of particle morphology and size distribution on the powder flowability and laser powder bed fusion manufacturability of Ti-6Al-4V alloy”. Additive Manufacturing, 31, pp. 544–548. https://doi.org/10.1016/j.addma.2019.100929.
[24] Wei, W. H., Wang, L. Z., Chen, T., Duan, X. M., and Li, W., 2017. “Study on the flow properties of ti-6al-4v powders prepared by radio-frequency plasma spheroidization”. Advanced Powder Technology, 28(9), pp. 2431–2437. https://doi.org/10.1016/j.apt.2017.06.025.
[25] Tan, J. H., Wong, W. L. E., and Dalgarno, K. W., 2017. “An overview of powder granulometry on feedstock and part performance in the selective laser melting process”. Additive Manufacturing, 18, pp. 228–255. https://doi.org/10.1016/j.addma.2017.10.011. [26] Walton, O. R., 2008. “Review of adhesion fundamentals for micronscale particles”. KONA Powder and Particle Journal, 26, pp. 129–141. https://doi.org/10.14356/kona.2008012.
[27] Pleass, C., and Jothi, S., 2018. “Influence of powder characteristics and additive manufacturing process parameters on the microstructure and mechanical behaviour of inconel 625 fabricated by selective laser melting”. Additive Manufacturing, 24, pp. 419–431. https://doi.org/10.1016/j.addma.2018.09.023.
[28] Madian, A., Leturia, M., Ablitzer, C., Matheron, P., Bernard-Granger, G., and Saleh, K., 2020. “Impact of fine particles on the rheological properties of uranium dioxide powders”. Nuclear Engineering and Technology, 52(8), pp. 1714–1723. https://doi.org/10.1016/j.net.2020.01.012.
[29] Weaver, J. S., Whiting, J., Tondare, V., Beauchamp, C., Peltz, M., Tarr, J., Phan, T. Q., and Donmez, M. A., 2021. “The effects of particle size distribution on the rheological properties of the powder and the mechanical properties of additively manufactured 17-4 ph stainless steel”. Additive Manufacturing, 39. https://doi.org/10.1016/j.addma.2021.101851.
[30] Nan, W., Ghadiri, M., and Wang, Y., 2017. “Analysis of powder rheometry of ft4: Effect of particle shape”. Chemical Engineering Science, 173, pp. 374–383. https://doi.org/10.1016/j.ces.2017.08.004.
[31] Vivacqua, V., L´opez, A., Hammond, R., and Ghadiri, M., 2019. “Dem analysis of the effect of particle shape, cohesion and strain rate on powder rheometry”. Powder Technology, 342, pp. 653–663. ttps://doi.org/10.1016/j.powtec.2018.10.034.
[32] Klein, A., and Clayton, J., 2019. “Developing an effective metal powder specification for Binder Jet Additive Manufacturing”. Metal AM, 5(2), pp. 151–157.
[33] Brika, S. E., Letenneur, M., Dion, C. A., and Brailovski, V., 2020. “Influence of particle morphology and size distribution on the powder flowability and laser powder bed fusion manufacturability of Ti-6Al-4V alloy”. Additive Manufacturing, 31. https://doi.org/10.1016/j.addma.2019.100929.

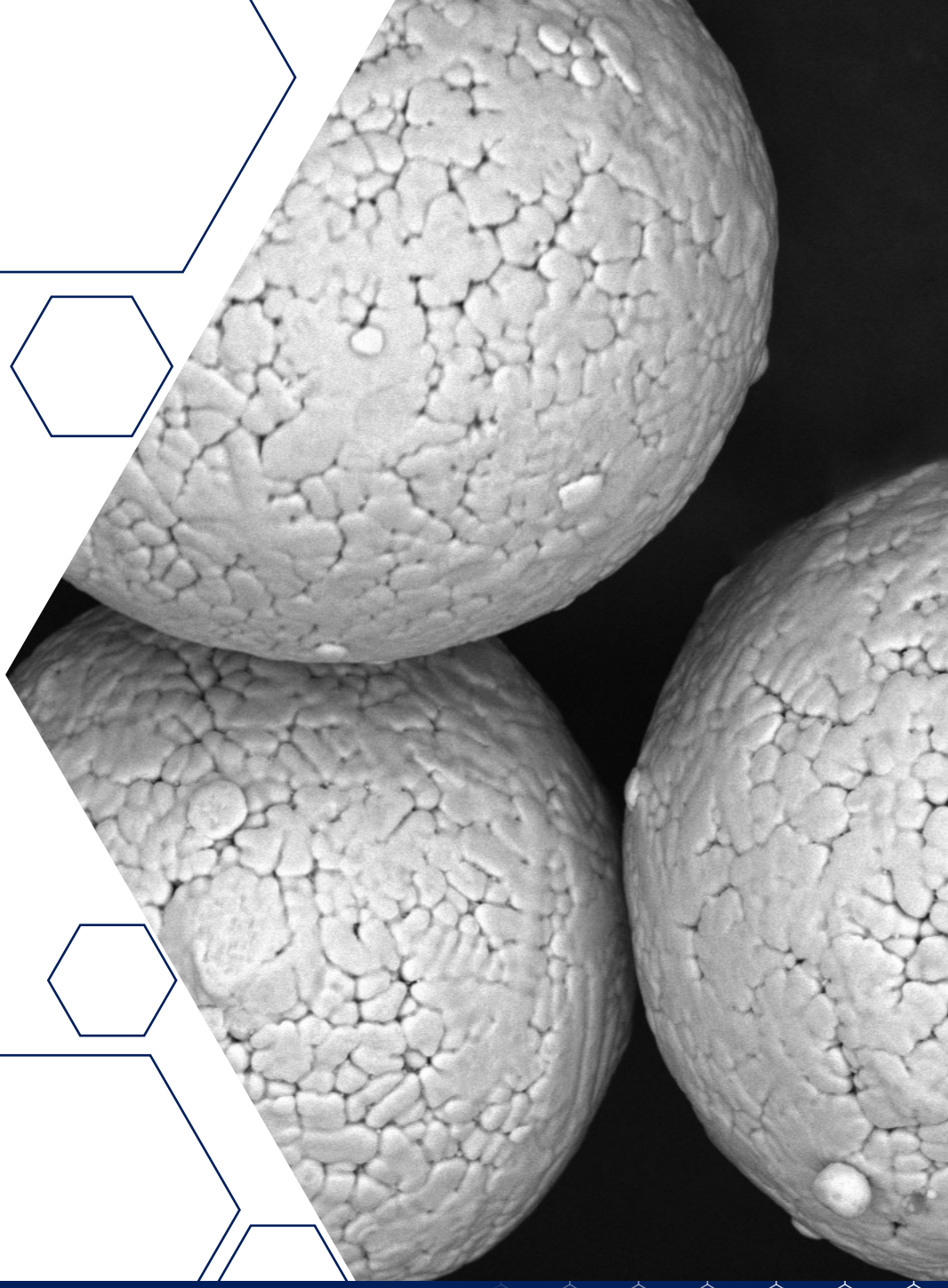

Particle Flow and Tribology Lab

RICE

C. Fred Higgs III Ph.D.
George R. Brown School of Engineering
6100 Main St. Houston, TX 77005